Heliyon

ELSEVIER

Received:
15 May 2018
Revised:
11 August 2018
Accepted:
11 October 2018

Cite as: Nashrulhaq Tagiling, Raizulnasuha Ab Rashid, Siti Nur Amirah Azhan, Norhayati Dollah, Moshi Geso, Wan Nordiana Rahman. Effect of scanning parameters on dose-response of radiochromic films irradiated with photon and electron beams. Heliyon 4 (2018) e00864. doi: 10.1016/j.heliyon.2018.e00864

Effect of scanning parameters on dose-response of radiochromic films irradiated with photon and electron beams

Nashrulhaq Tagiling [a], Raizulnasuha Ab Rashid [a], Siti Nur Amirah Azhan [a], Norhayati Dollah [b], Moshi Geso [c], Wan Nordiana Rahman [a,*]

[a] *Medical Radiation Programme, School of Health Sciences, Universiti Sains Malaysia (Health Campus), Kelantan, Malaysia*

[b] *Department of Nuclear Medicine, Radiotherapy and Oncology, Hospital Universiti Sains Malaysia (HUSM), Kelantan, Malaysia*

[c] *Division of Medical Radiation, School of Health and Biomedical Sciences, RMIT University, Bundoora, Victoria, Australia*

[*] Corresponding author.

E-mail address: wandiana@usm.my (W.N. Rahman).

Abstract

Proper dosimetry settings are crucial in radiotherapy to ensure accurate radiation dose delivery. This work evaluated scanning parameters as affecting factors in reading the dose-response of EBT2 and EBT3 radiochromic films (RCFs) irradiated with clinical photon and electron beams. The RCFs were digitised using Epson® Expression® 10000XL flatbed scanner and image analyses of net optical density (*netOD*) were conducted using five scanning parameters i.e. film type, resolution, image bit depth, colour to grayscale transformation and image inversion. The results showed that increasing spatial resolution and deepening colour depth did not improve film sensitivity, while grayscale scanning caused sensitivity reduction below than that detected in the Red-channel. It is also evident that invert and colour negative film type selection negated *netOD* values, hence unsuitable for scanning RCFs. In conclusion, choosing appropriate

https://doi.org/10.1016/j.heliyon.2018.e00864

scanning parameters are important to maintain preciseness and reproducibility in films dosimetry.

Keyword: Nuclear physics

1. Introduction

The commercially available GAFCHROMIC™ (Ashland Specialty Ingredients, Bridgewater, NJ, USA) radiochromic films or RCFs were developed as a 2-D chemical-based dosimeter for radiation measurements and verification in radiotherapy. It relies on solid-state polymerisation upon exposure to ionising radiation, triggering a permanent colour change to occur [1]. The first variant of GAFCHROMIC™ EBT films was first launched in 2004 but has been discontinued in favour of EBT2. As a successor of the original film model, EBT2 was developed with an addition of yellow marker dye into the active layer (lithium salt of pentacosa-10, 12-diynoic acid or LiPCDA). This improves film response discrepancies created by the domination of signal in the green and red spectrum [2]. The third-generation film, namely EBT3 has the identical active layer chemical compound and thickness as its predecessor. Its symmetrical design is an upgrade from the asymmetrical EBT2 (different thickness of layers), which is shown to be dependent towards scanning side [3]. Both EBT3's matte polyester foils' surfaces were embedded with fine silica particles to prevent the formation of Newton's Rings. Notable benefits of RCFs other than being user-friendly include high spatial resolution, weak energy dependence across multiple beam modalities, capable of fractionated dose measurements and submergible in aqueous solution for niche dosimetry applications.

The properties and performances of these two film types have been the subject of research in the past. Film characterisation, for example, was interpolated by a number of analytical functions, one of which is quantifying the change in optical density (*netOD*) against prescribed dose [4, 5, 6, 7, 8]. Whilst establishing dose-response or calibration curve fitting has been discussed in recent studies, no unanimity has been attained by scholars on an ideal equation because each has its own inherent edge and limitation [2, 9, 10, 11].

Another significant aspect of film dosimetry is optimum scanning preferences in scanning protocols. Since the rise of flat-bed scanners for RCFs digitisation, multiple scanning software parameters have been listed out as defaults to prevent any unnecessary alterations in establishing the relationship of film darkening and prescribed dose. However, few attempts had been done by researchers to determine the effects of these parameters in a single study and most of the studies were done using only one type of RCF. To nail down the gap, this study set out to investigate five scanning variables (film type, resolution, image bit depth, colour to grayscale transformation

https://doi.org/10.1016/j.heliyon.2018.e00864

and image inversion) and assess the *netOD* dissimilarities from a scanning standard in the GAFCHROMIC™ EBT2 and EBT3 films. Two forms of mathematical equations are applied to analyse the datasets and to compare the response behaviour for EBT2 and EBT3 in photon and electron radiation beams.

2. Materials and methods

2.1. Film preparation and irradiation setup

Eighty-eight GAFCHROMIC™ film pieces of 3 cm × 3 cm in dimension were utilised for this experiment. One batch of forty-four film pieces were cut from GAFCHROMIC™ EBT2 film sheets (Lot #A09271203), while another batch of the same amount were cut from GAFCHROMIC™ EBT3 film sheets (Lot #A05151201). Film care throughout the work, such as storage and orientation tracking were in accordance with the American Association of Physicists in Medicine (AAPM) TG-55 report [12]. Irradiations were achieved by using a PRIMUS™ Linear Accelerator (Siemens Medical Systems, Concord, CA, USA) at Hospital Universiti Sains Malaysia (HUSM). The categorisation of the film pieces was done in four groups of radiation energy per RCF model (1: 6 MV, 2: 10 MV, 3: 6 MeV, 4: 9 MeV). Films from each of the allocated groups were placed at different depths of maximum dose (D_{max}), inside a 15 cm thick and 30 cm × 30 cm solid water phantom (PTW-Freiburg, Freiburg, Germany). D_{max} of each beam energies are as follows: 6 MV = 1.5 cm, 10 MV = 2.5 cm, 6 MeV = 1.4 cm and 9 MeV = 2.3 cm. The entire measurements were executed with a field size of 10 cm × 10 cm and source-to-surface distance (SSD) of 100 cm. To create response curves, each film groups were irradiated with ten dose levels in steps of 0.5 Gy, stretching from 0.5 Gy to 5.0 Gy. Considering continuous polymerisation of active layer post-irradiation, scanning was conducted a day after in conformity to the 24 hours protocol [13].

2.2. Scanning and image processing

An Epson® Expression® 10000XL flatbed scanner (Epson Seiko Corp., Nagano, Japan) was used for this study. The scanner is equipped with a transparency unit for transmission mode, which is the recommended mode for RCF scanning [3]. Digitisation of films were made using PTW FilmScan software version 2.8. (PTW-Freiburg, Freiburg, Germany), and is TWAIN Driver compatible for operability with Epson's own scanning driver. Film pieces were handled individually with gloves and cleaned using 70% ethanol solution, and wiped with a soft microfiber cloth to avoid systematic errors during handling. To ensure minimal scanner response uncertainty or lateral artefact, measurements were made prior to scanning to determine the scanner bed's central region, and each of the film pieces was positioned strategically

https://doi.org/10.1016/j.heliyon.2018.e00864

on it. The scanner was then switched on 15 to 30 minutes prior to scanning activities in order to warm up the electronics [14].

Scanning software is usually equipped with multiple parameters that act as tools to aid users in obtaining the desired image. Five scanning parameters that were found extensively in the literature were employed in this investigation: film type, resolution, image bit depth, colour to grayscale transformation and image inversion. The definition and description of each parameter used were tabulated in Table 1. Three preview scans were made to stabilise the scanner lamp output, and all image adjustments, colour corrections, flattening corrections and lookup tables were disabled and reset to ensure the final image is optimised for display. To scan the films using default parameters, positive film type of 72 dots per inch (dpi) resolution in true colour 24-bit Red-Green-Blue (RGB) with no image inversion were registered into the software. The default image was then converted and analysed in Red-channel because it possesses the highest sensitivity among the RGB channels and most accurate to the tested dose interval which is below 8 Gy [15]. The remaining experimental scans were fine-tuned from the properties summarised in Table 1. All images were saved as tagged image file format (.tiff).

Changes in optical density for each dose point were calculated using pixel value of reflected intensity (I) readouts. FilmCal software version 2.4. (PTW-Freiburg, Freiburg, Germany) was used to extract I, and samplings were obtained from three

Table 1. Scanning parameters tested for EBT2 and EBT3 film calibration.

Parameter	Description	Default	Experimental
Film type	Type of photographic material	Colour positive: Film showing photographic image with tones corresponding to the original subject	Colour negative: Film showing photographic image with reversed tones
Resolution	Image detailing	72 dpi: Low resolution	300 dpi: High resolution 600 dpi: High resolution
Image bit depth	Number of stored colour information	24-bit RGB: 16.8 million colour information; 8-bit per colour channel	48-bit RGB: 281 trillion colour information; 16-bit per colour channel 16-bit Grayscale: 65, 536 levels of grey shades
Colour to grayscale transformation	Conversion of RGB to grayscale	Red-channel: Grayscale image formed by the red component of an RGB image	$Y'C_BC_R$ grayscale (luma): Grayscale image of gamma-corrected RGB colour space
Image inversion	Change of pixel value	No invert: Image retains its pixel values	Invert: Image inverts its pixel values

https://doi.org/10.1016/j.heliyon.2018.e00864

similar Region-of-Interest (ROI) on each scanned image using a feature called Average Region [16], to verify exposure homogeneity. The calculation of netOD was achieved by using Eq. (1):

$$netOD = OD_{exp} - OD_{unexp} = log_{10}\left(\frac{I_{unexp}}{I_{exp}}\right) \tag{1}$$

I_{unexp} represents the averaged pixel value of the reflected intensity in unexposed film pieces and I_{exp} relates to the averaged pixel value of the reflected intensity exposed film pieces according to the dose prescribed for irradiation. Uncertainties in the *netOD* values were determined by the standard deviation of the mean pixel values obtained from the ROI, shown as error bars. The formula was:

$$\sigma_{netOD} = \frac{1}{\ln(10)} \cdot \sqrt{\left(\frac{\sigma_{I_{unexp}}}{\sigma_{I_{unexp}}}\right)^2 + \left(\frac{\sigma_{I_{exp}}}{\sigma_{I_{exp}}}\right)^2} \tag{2}$$

where $\sigma_{I_{unexp}}$ and $\sigma_{I_{exp}}$ are the standard deviation of the measured I_{unexp} and I_{exp}.

2.3. Dose-response analysis

Response curves were plotted from *netOD* against dose (Gy). Soares *et al* [17] reported that second-order (quadratic) and third-order (cubic) polynomial function provided sufficient accurate fit for film dosimeter characterisation. In order to choose the best fit for the evaluated datasets, it is decided to compare Eq. (3) by Devic *et al* [4] in the form of quadratic and cubic. The fitting functions investigated were given in the analytical form of:

$$D = B \cdot netOD + C \cdot netOD^n \tag{3}$$

$$D = B \cdot netOD + C \cdot netOD^2 \tag{4}$$

$$D = B \cdot netOD + C \cdot netOD^3 \tag{5}$$

B and C were fitting parameters and the power of n was introduced on the basis of non-linear saturation of RCF at high doses. The n value was fixed to 2.0 and 3.0 to resemble the quadratic and cubic function accordingly. Orthogonal Distance Regression (ODR) algorithm was used for fitting instead of the generally used least square method of Levenberg-Marquardt (LM) algorithm within the Nonlinear Curve Fit option of OriginPro 2018 software (OriginLab, Northampton, MA). This form of regression enables evaluation of uncertainties for independent variables through the minimisation of the sum of squared orthogonal distances between each data point and the fitted curve [18].

https://doi.org/10.1016/j.heliyon.2018.e00864

Quantitative analyses of each response curve were completed by measuring their relative differences (R_{diff}). The formula for relative difference percentage between *netOD* was expressed in Eq. (6):

$$R_{diff}\ (\%) = \left(\frac{netOD_{def} - netOD_{test}}{netOD_{def}}\right) \cdot 100 \tag{6}$$

Values for $netOD_{def}$ and $netOD_{test}$ relates to the *netOD* measurement of default scan and parameter testing scan accordingly. Assessments for all graphs were made along a 0.5 Gy grid of prescribed dose (x-axis) in all energy levels.

3. Results

3.1. Film preparation and irradiation setup

The first point of best-fit consideration was done through visual inspection. Fig. 1(A) and (B) show the dose-response under default scanning parameters. Upon review of characteristic curvatures in all of the beam qualities, net optical densities in EBT3 were found to be higher than EBT2 because of the layering changes from older to newer RCF model [19]. Both fitting Eqs. (4) and (5) provided smooth fit shapes. No Runge's Phenomenon or oscillatory tendencies were exhibited between data points by Eq. (5) which is commonly seen in higher polynomial order [20, 21]. The modified quadratic and modified cubic equations had also been applied for fitting suitability comparison using OriginPro's built-in functionality of conducting Akaike's Information Criterion (AIC) Test. The outcomes are conclusive as all data-sets fitted with the modified quadratic equation displayed lower AIC, hence more likely to be correct.

Computations of reduced chi-square ($\tilde{x}^2$) were made as the final indicator for goodness-of-fit. Results from the two calibration equations were placed side by side and as shown in Table 2, smaller $\tilde{x}^2$ values were observed for the quadratic function in both beam qualities. Seeing that the outcome was in support of Eq. (4), the

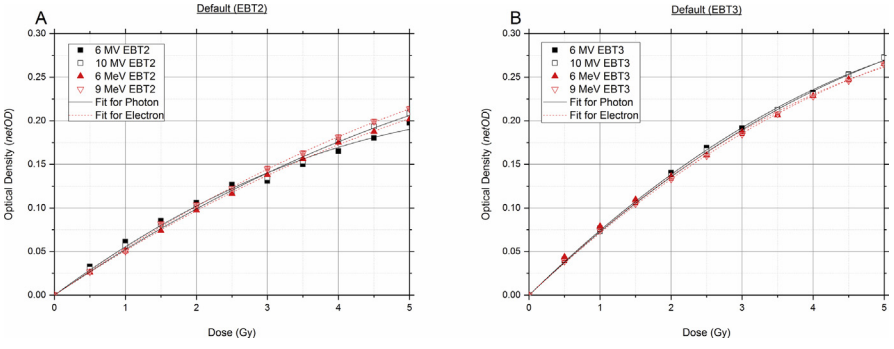

Fig. 1. Default dose-response curves of irradiated EBT2 films (A) and EBT3 films (B) for photon and electron beams.

https://doi.org/10.1016/j.heliyon.2018.e00864

Table 2. Fitting analysis values according to reduced chi-square ($\tilde{x}^2$).

Film type	Function, *n*	6 MV (10^{-5})	10 MV (10^{-5})	6 MeV (10^{-5})	9 MeV (10^{-5})	Averaged photon (10^{-5})	Averaged electron (10^{-5})
EBT2	2	3.35	1.41	0.12	0.35	2.09	0.11
	3	6.26	2.56	0.16	0.60	4.01	0.25
EBT3	2	0.61	0.50	1.43	0.28	0.50	0.70
	3	2.38	2.03	4.11	1.65	2.15	2.71

equation was then used for every follow-up curve fitting in this study. Error bars of the measured *netOD* values are smaller than the markers, thus barely visible in each of the graphs. The average standard deviations of *netOD* obtained from Eq. (2) in EBT2 and EBT3 films for all of the evaluated parameters including the default parameters were found to be consistent at less than 0.2%. Plus, the coefficient of determination (R^2) and its adjusted value (R^2_{adj}) was equal to 1 in all of the dose-response curves, indicating an appropriate fit.

3.2. Film type

Distinct changes were observed during the colour negative film scan on RCFs. Fig. 2(A) illustrates EBT2 characteristic graph between positive and negative film

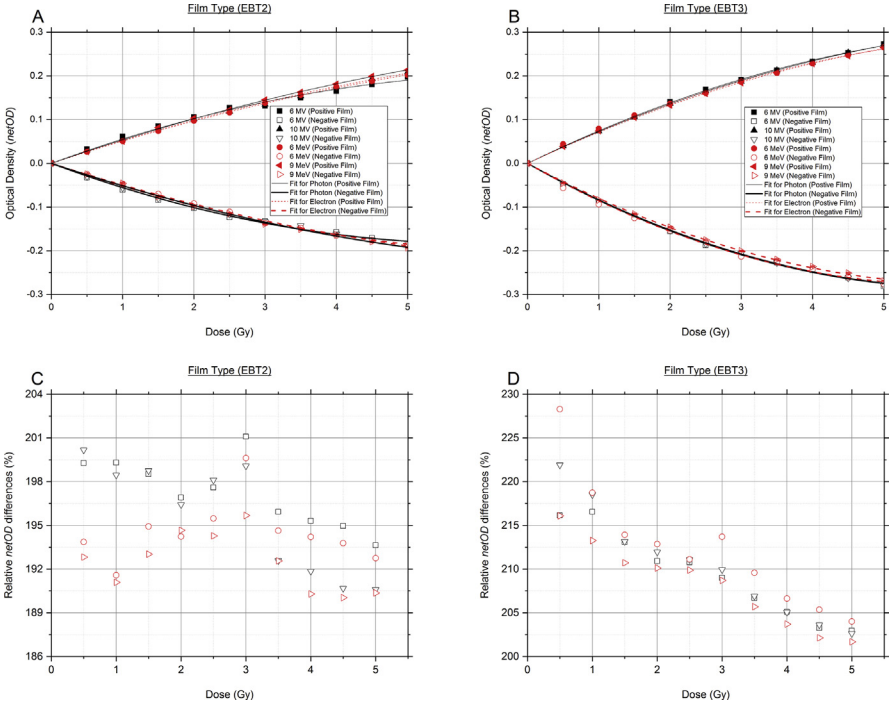

Fig. 2. Dose-response comparison of colour positive and colour negative film type parameter for EBT2 and EBT3 films (A, B) with the corresponding relative *netOD* difference percentages (C, D) across four beam energies.

https://doi.org/10.1016/j.heliyon.2018.e00864

scanning. The dose-response curve for a positive film image rose in a non-linear orientation which is expected and normally observed. However, negative optical density values due to the selection of negative film in the scanning software cause the curve to manifest a mirror-like response, which is counterintuitive to the default. The same results can be seen in EBT3 films in Fig. 2(B). Graphical representations of relative *netOD* difference percentages were presented in Fig. 2(C) and (D). The mean relative differences of negative film with respect to positive film in EBT2 and EBT3 were 137.7% and 150.1%, respectively. Thus, it is imperative to be wary of always selecting positive film type prior to digitising the film pieces.

3.3. Resolution

Outcomes of different scanning spatial resolution were charted and superimposed on the default dose-response curve in Fig. 3(A) and (B). Despite the similar curve trend, values for *netOD* in each dose points were seen to be minutely inconsistent across the scanning resolutions. Fig. 3(C) and (D) show the relative difference percentages for different resolution scans of RCFs throughout 6 MV, 10 MV, 6 MeV and 9 MeV irradiations. Observation of R_{diff} for EBT2 shows a relative difference in the range of 0.01% to 1.60%, with the exception of few points at a dose of 50 cGy, which shows percentages reaching up to 4%. The tested EBT3 film lot also shows a similar range of relative difference percentage, varying between 0.01% and 1.70%. One possible

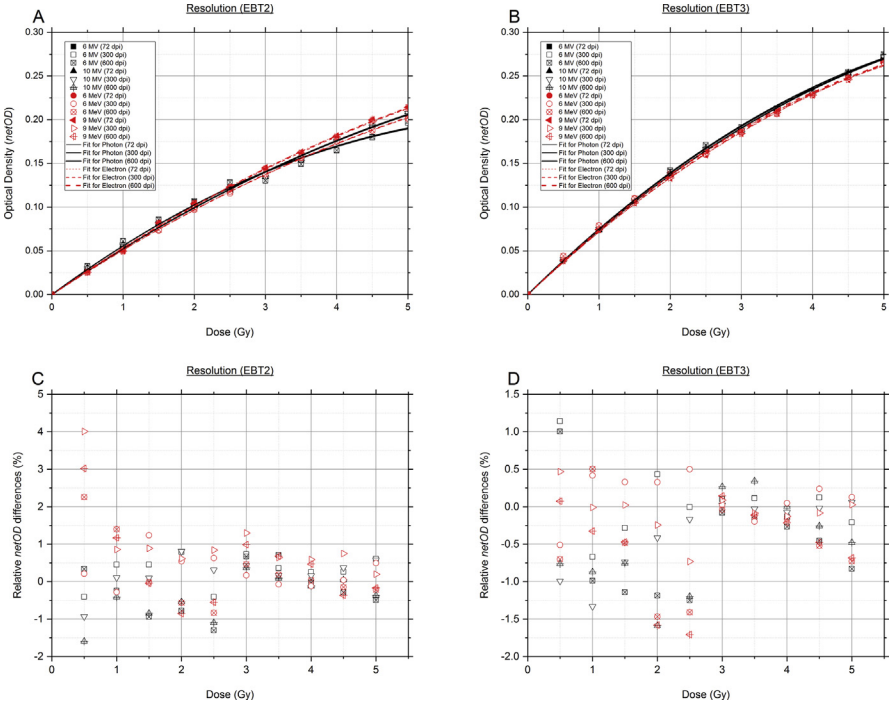

Fig. 3. Dose-response comparison of three spatial resolutions for EBT2 and EBT3 films (A, B) with the corresponding relative *netOD* difference percentages (C, D) across four beam energies.

https://doi.org/10.1016/j.heliyon.2018.e00864

reasoning behind the minor irregularities in *netOD* values may be due to noise corruption that has affected the sampling of *I*.

3.4. Image bit depth

Three image types were weighed against each other in Fig. 4. In both cases of photon and electron irradiation, 24-bit RGB and 48-bit RGB scans did not show any significant differences in their respective response curves, with a median relative difference percentage of 0.58% for EBT3 films (Fig. 4(B)) and 1.21% for EBT2 films (Fig. 4(A)). Colour bit depth images of both 24-bit and 48-bit produced noticeably higher net optical density reading, causing the characteristic curve to be higher than its grayscale counterpart of 16-bit. The mean R_{diff} percentages of 16-bit grayscale drawn from Fig. 4(C) for EBT2 and Fig. 4(D) for EBT3 are 18.9% and 27.8% respectively.

3.5. Colour to grayscale transformation

Predefined $Y'C_BC_R$ grayscale encoding (luma) was compared against the Red-channel in Fig. 5. Close examination of the findings in this testing shows luma to exhibit a nearly identical response to 16-bit grayscale from the previous section. The mean relative difference percentage of luma and Red-channel is 14.8% for

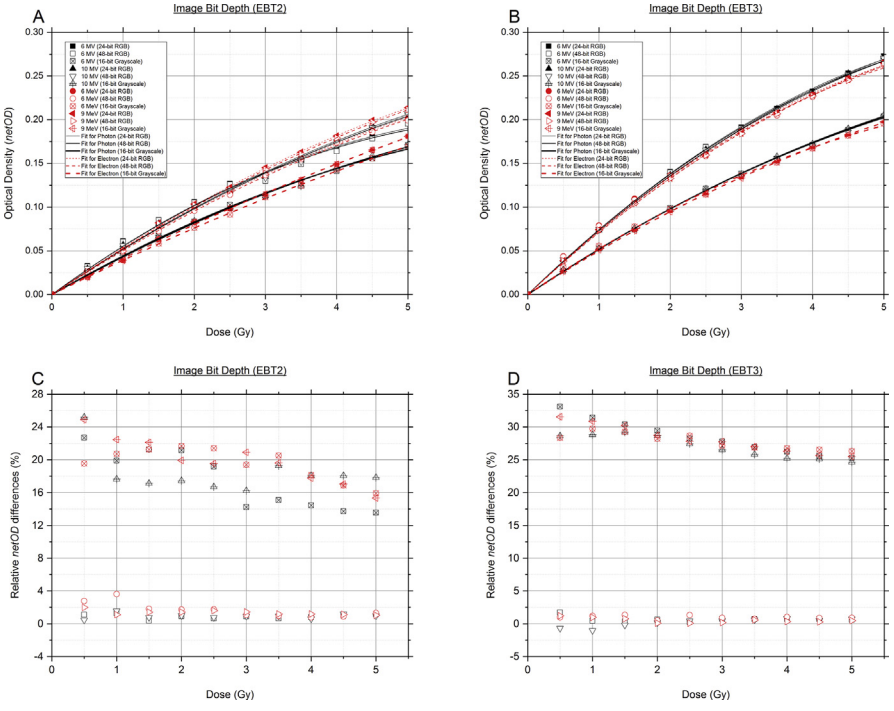

Fig. 4. Dose-response comparison of three different image bit depths for EBT2 and EBT3 films (A, B) with the corresponding relative *netOD* difference percentages (C, D) across four beam energies.

https://doi.org/10.1016/j.heliyon.2018.e00864

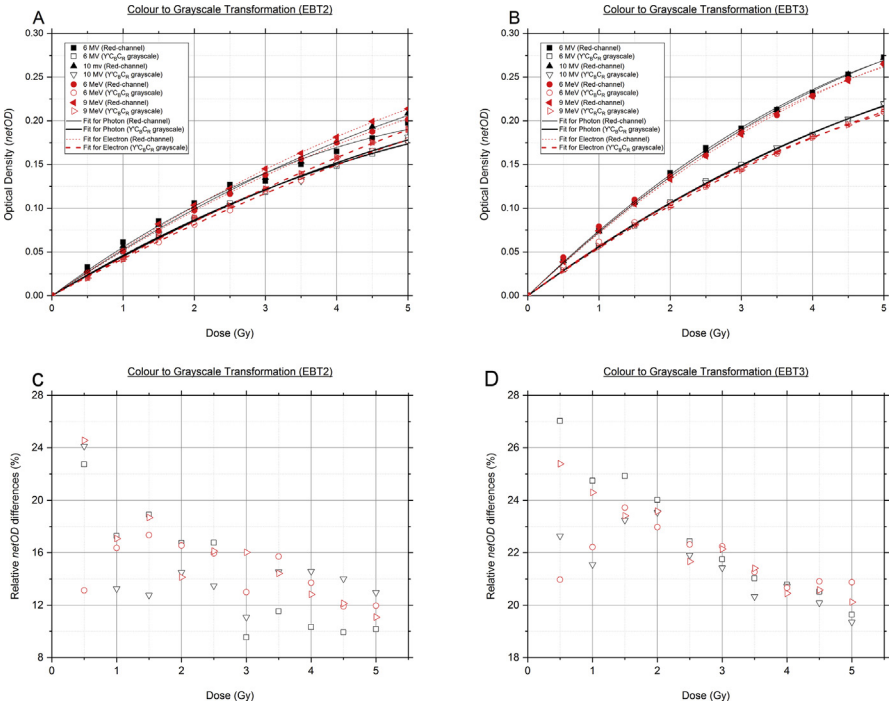

Fig. 5. Dose-response curves of colour to grayscale transformation and its *netOD* R_{diff} percentages for EBT2 films (A, C) and EBT3 films (B, D) in photon and electron beams.

EBT2 (Fig. 5(C)), while EBT3 (Fig. 5(D)) is 22.1%. The result provided proof that Red-channel is higher in sensitivity across the dose range in comparison to luma, but less wide in terms of film dynamic range response.

3.6. Image inversion

Another obvious dose-response incongruity similar in behaviour to the results identified in colour negative film type was spotted in Fig. 6 of image inversion testing. Applying invert onto default images of 24-bit RGB produces a *netOD* reading that deviates to the negative region as shown in Fig. 6(A) and (B). The parameter had introduced relative difference percentage values up to 144% in EBT2 (Fig. 6(C)) and 164% in EBT3 (Fig. 6(D)). Users are advised to keep constant interpretation setting throughout the RCF scanning process to ensure cohesive image analysis.

4. Discussion

Optimisation of film characterisation in each radiation and scanning modality were accomplished independently as recommended for each RCF lot by using calibration fits to gain the best dosimetric expression. The use of Eq. (3) as a form of fitting function for RCF calibration curves can be traced back to a study devised by Devic *et al* [22], where they tested varying numbers of n between 0.5 to 5.0 for

https://doi.org/10.1016/j.heliyon.2018.e00864

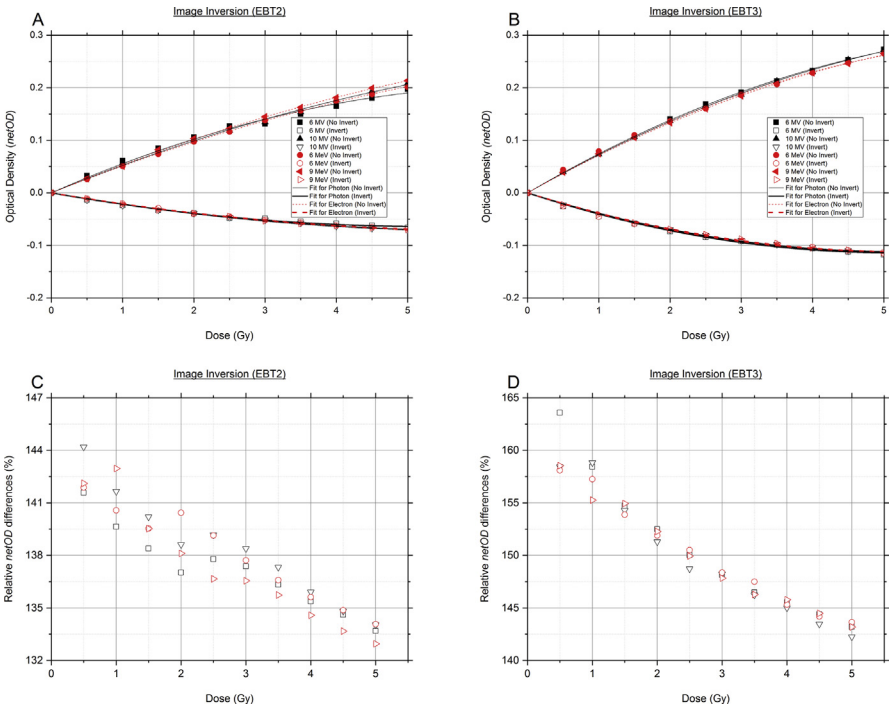

Fig. 6. Dose-response curves of image inversion and its *netOD* R_{diff} percentages for EBT2 films (A, C) and EBT3 films (B, D) in photon and electron beams.

GAFCHROMIC™ High Sensitivity (HS) and XR-T using seven different densitometers. Less than a year later, Devic *et al* [4] reported a value of $n = 2.5$ for HS and EBT film, scanned using Agfa Arcus II (Agfa-Gevaert N.V., Mortsel, Belgium) scanner. Comparison of EBT2 and EBT3 film batches for clinical photon and proton by Reinhardt *et al* [8] showed n varies from 2.4 to 2.9. Other published papers fixed the exponent n to 3.1 for EBT3 scanning with Epson® Expression® 10000XL [5] and obtained $n = 2.0$ for EBT3 digitisation using Epson® Perfection® V750 Pro [6].

Diverse values of n across literature can be justified by the difference in RCF type, film lot, and densitometer combination. Despite similar setup pairing to one of the prior studies [5], the result turns out to be inconsistent. Selection of $n = 2.0$ in the current study corroborates with the findings by Castriconi *et al* [6], which was handled using a different densitometer. Further comparative examination made on Epson scanners quality for RCF evaluation suggested V700 scanner series used by the last-mentioned study [6] is commensurable in providing similar quality and accuracy as the 10000XL [23]. Thus, it is possible to infer that $n = 2.0$ can be used for EBT2 and EBT3 scanning in both types of Epson scanners.

Low scanning resolution has been reported to improve dose reading accuracy, and it has been suggested that 72−75 dpi provides fair settlement between image resolution and noise [14, 24] although high resolution noise contribution can be minimised by averaging multiple scans of each film [2]. Data shown in the resolution

https://doi.org/10.1016/j.heliyon.2018.e00864

investigation for EBT2 and EBT3 combined indicates that no more than 2% of R_{diff} percentage values were above the 2% mark. Other advantages of choosing smaller resolution might include smaller image file size and quicker scanning time due to lesser working memory requirement. However, Chiu-Tsao *et al* [25] argued that a sharper resolution of 300 dpi would be crucial for brachytherapy and other small field applications (stereotactic radiosurgery, stereotactic body radiation therapy) as an accurate dose distribution measurement are highly demanded.

Experimental evidence for GAFCHROMIC™ EBT2 and EBT3 films in this study shows that no identifiable plus point could be given by increasing the colour bit depth to 48-bit RGB. Only 3 points of the relative *netOD* differences out of 160 points in Fig. 4(C) and (D) altogether were above 2% and it is exclusively observed in EBT2 and may occur due to electronic noise during image acquisition. Conclusions asserted by earlier studies using RGB images had clearly discussed that bit depth did not influence the sensitivity of RCF reading [14, 26]. Low-cost charge-coupled device (CCD) in commercial document scanners such as Epson® Expression® 10000XL had been identified as a key barrier for detecting beneficial out-turn in higher bit depth RCF scanning. The CCDs were known to have low dynamic range and was found to be incapable of detecting useful signal other than noise in the 48-bit RGB scans. A note of caution is needed upon grayscale mode scans as they became lower in response. These results reflect those of Alva *et al* [27] who also found the similar condition of 8-bit grayscale under response in GAFCHROMIC™ MD-55 film. Strategy to overcome this issue is to continually use RGB during scanning regiment. RGB images are known for its manipulability into three colour channels in contrast to grayscale images. To provide a complete picture of the RCFs' dynamic range, further work needs to be undertaken by using higher dose intervals for analysis with other colour channels (Green and Blue-channel).

PTW provided a brief description of their automated RGB conversion to grayscale method upon scanning via colour to grayscale transformation setting in the TWAIN tab [16]. It allows grayscale conversion to be made according to custom RGB weighting factors. Luma is described as gamma-corrected RGB colour space and the $0.299R + 0.587G + 0.114B$ conversion weighting was formed to account human eye perception on certain wavelengths of light [28]. Since data from this testing is comparable with 16-bit Grayscale scans (both are grayscales), the comparison between the dose-response of both types was diagrammed in Fig. 7. Looking at Fig. 7(A) and (B), we can see that luma has a higher characteristic curve, hence more sensitive compared to 16-bit grayscale. The observed increase in *netOD* may be explained by the fact that both have different grayscale conversion approaches. One can assume that 16-bit Grayscale uses either Lightness or Average grayscale conversion method [28], with the latter being the simplest.

Although this is not a correct RCF scanning procedure, choosing colour negative film causes the computer code to develop image output mimicking photographic

https://doi.org/10.1016/j.heliyon.2018.e00864

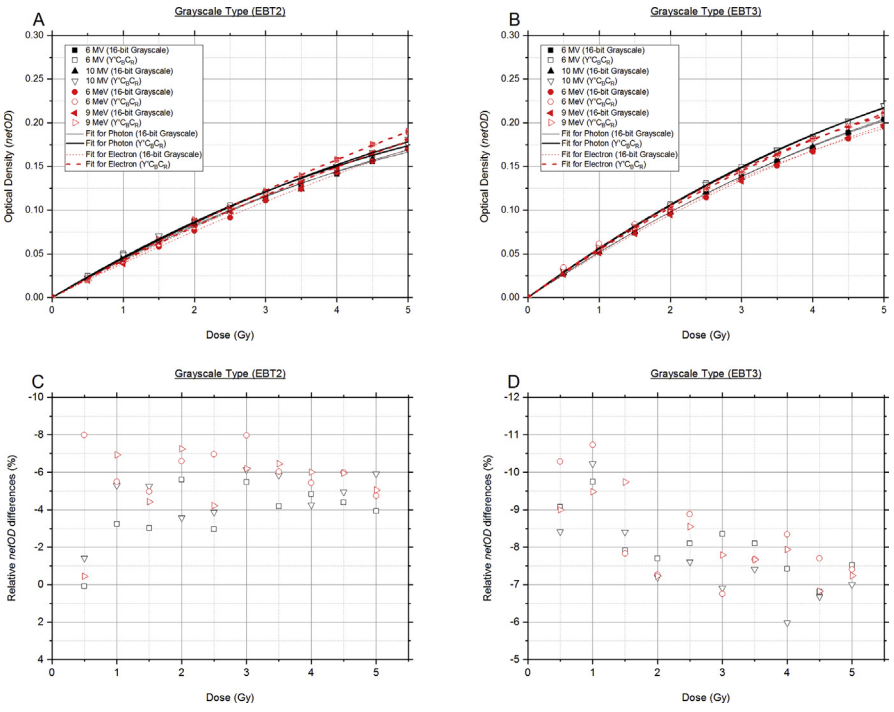

Fig. 7. Dose-response curves of grayscale type and its *netOD* R_{diff} percentages for EBT2 films (A, C) and EBT3 films (B, D) in photon and electron beams.

negative state. This is attributable to a basic image processing called negative grayscale linear enhancement [29]. Low pixel values (dark) in a grayscale image were switched to high values (bright) and vice versa through an algorithmic program implemented by the scanner software. The invert tool also produces the same effect; but despite having the same 'feature', the results displayed were visually different as invert creates a lower pixel value (darker) around the film area, hence showing higher I_{unexp} and I_{exp} values than colour negative. One possible explanation for this occurrence was a different negative grayscale enhancement algorithm working in the background.

5. Conclusion

In summary, this study is designed to investigate the effects of image acquisition parameters and indicate guidelines for future radiochromic film scanning. Dose-response analysis for EBT2 and EBT3 shows parallel results in best curve fit and all scanning parameters tested for photon and electron irradiations. The present research has demonstrated and reassured that scanning a 24-bit RGB image with low spatial resolution in Red-channel component provides sufficient and optimal conditions for film calibration. The major distinction in characteristic curves caused by negative film and invert parameter must be discarded and rescanning should be run by following standard scanning procedures. These findings provide strong

https://doi.org/10.1016/j.heliyon.2018.e00864

empirical confirmation that maintaining an appropriate scanning parameter is a priority for overall precision and reproducible film dosimetry routine across all types of RCF in radiotherapy centres.

Declarations

Author contribution statement

Nashrulhaq Tagiling: Conceived and designed the experiments; Performed the experiments; Analyzed and interpreted the data; Contributed reagents, materials, analysis tools or data; Wrote the paper.

Raizulnasuha Ab Rashid, Siti N. A. Azhan, Norhayati Dollah: Conceived and designed the experiments; Performed the experiments; Contributed reagents, materials, analysis tools or data.

Moshi Geso: Analyzed and interpreted the data.

Wan N. Rahman: Conceived and designed the experiments; Analyzed and interpreted the data; Contributed reagents, materials, analysis tools or data.

Funding statement

This work was supported by Universiti Sains Malaysia Research University Grant (RUI: 1001/PPSK/8012212) and Short Term Grant (304/PPSK/61313139).

Competing interest statement

The authors declare no conflict of interest.

Additional information

No additional information is available for this paper.

Acknowledgements

The authors wish to thank the staffs of Nuclear Medicine, Radiotherapy and Oncology Department of Hospital Universiti Sains Malaysia (HUSM) for helping in conducting irradiations for this experiment.

References

[1] W.L. McLaughlin, M. AlSheikhly, D.F. Lewis, A. Kovacs, L. Wojnarovits, Radiochromic solid-state polymerization reaction, ACS Sym. Ser. 620 (1996) 152−166.

https://doi.org/10.1016/j.heliyon.2018.e00864

[2] I.J. Das, Radiochromic Film Role and Applications in Radiation Dosimetry, CRC Press, Boca Raton, FL, 2018, 386 p.

[3] J. Desroches, H. Bouchard, F. Lacroix, Potential errors in optical density measurements due to scanning side in EBT and EBT2 Gafchromic film dosimetry, Med. Phys. 37 (4) (2010) 1565−1570.

[4] S. Devic, J. Seuntjens, E. Sham, E.B. Podgorsak, C.R. Schmidtlein, A.S. Kirov, et al., Precise radiochromic film dosimetry using a flat-bed document scanner, Med. Phys. 32 (7) (2005) 2245−2253.

[5] J. Sorriaux, A. Kacperek, S. Rossomme, J.A. Lee, D. Bertrand, S. Vynckier, et al., Evaluation of Gafchromic(R) EBT3 films characteristics in therapy photon, electron and proton beams, Phys. Med. 29 (6) (2013) 599−606.

[6] R. Castriconi, Response of EBT3 Radiochromic Film Dosimeters to Proton and Carbon Ion Hadrontherapy Beams [Electronic], University of Naples Federico II, Naples, Italy, 2016. www.infn.it/thesis/PDF/getfile.php?filename=10202-Castriconi-magistrale.pdf.

[7] M. Najafi, G. Geraily, A. Shirazi, M. Esfahani, J. Teimouri, Analysis of Gafchromic EBT3 film calibration irradiated with gamma rays from different systems: gamma knife and cobalt-60 unit, Med. Dosim. 42 (3) (2017) 159−168.

[8] S. Reinhardt, M. Hillbrand, J.J. Wilkens, W. Assmann, Comparison of Gafchromic EBT2 and EBT3 films for clinical photon and proton beams, Med. Phys. 39 (8) (2012) 5257−5262.

[9] J.A. Martin-Viera Cueto, V. Parra Osorio, C. Moreno Saiz, F. Navarro Guirado, F.J. Casado Villalon, P. Galan Montenegro, A universal dose-response curve for radiochromic films, Med. Phys. 42 (1) (2015) 221−231.

[10] M. Tamponi, R. Bona, A. Poggiu, P. Marini, A new form of the calibration curve in radiochromic dosimetry. Properties and results, Med. Phys. 43 (7) (2016) 4435.

[11] L.B. Xu, Commissioning of a GafChromic EBT Film Dosimetry Protocol at Ionizing Radiation Standards Group of National Research Council, McGill University, Montreal, Québec, Canada, 2009. http://digitool.library.mcgill.ca/thesisfile67022.pdf.

[12] A. Niroomand-Rad, C.R. Blackwell, B.M. Coursey, K.P. Gall, J.M. Galvin, W.L. McLaughlin, et al., Radiochromic film dosimetry: recommendations of AAPM radiation therapy committee task group 55, Med. Phys. 25 (11) (1998) 2093−2115.

[13] T. Cheung, M.J. Butson, P.K. Yu, Post-irradiation colouration of Gafchromic EBT radiochromic film, Phys. Med. Biol. 50 (20) (2005) N281−N285.

https://doi.org/10.1016/j.heliyon.2018.e00864

[14] B.C. Ferreira, M.C. Lopes, M. Capela, Evaluation of an Epson flatbed scanner to read Gafchromic EBT films for radiation dosimetry, Phys. Med. Biol. 54 (4) (2009) 1073−1085.

[15] S.-W. Kang, J.-B. Chung, K.-H. Kim, K.-Y. Eom, C. Song, J.-W. Lee, et al., Evaluation of dual-channel compound method for EBT3 film dosimetry, Prog. Med. Phys. 28 (1) (2017) 16−21.

[16] PTW-Freiburg, User manual FilmCal, in: PTW-Freiburg (Ed.), Printed. 2.4 or Higher Ed, PTW-Freiburg, Freiburg, Germany, 2011, p. 11. http://www.ptw-usa.com/typo3conf/ext/naw_securedl/secure.php?u=0&file=ZmlsZWFkbWluL2ludGVybmFscy9yYWRfdGhlcmFweS9tYW5fc3BlYy9GaWxtQ2FsX1NXMi00X01hbl9lbl83NTExMzEwMF8wNC5wZGY=&t=1498185891&hash=8016e72fd94e2ff66a43612012aa300a.

[17] C.G. Soares, S. Trichter, S. Devic, Radiochromic Film. Clinical Dosimetry Measurements in Radiotherapy (AAPM 2009 Summer School Textbook), Medical Physics Publishing, Madison, WI, 2009, p. 1128.

[18] P.T. Boggs, R.H. Byrd, R.B. Schnabel, A stable and efficient algorithm for nonlinear orthogonal distance regression, SIAM J. Sci. Stat. Comput. 8 (6) (1987) 1052−1078.

[19] R. Dreindl, D. Georg, M. Stock, Radiochromic film dosimetry: considerations on precision and accuracy for EBT2 and EBT3 type films, Z. Med. Phys. 24 (2) (2014) 153−163.

[20] A. Peirce, Lecture 3: the Runge Phenomenon and Piecewise Polynomial Interpolation, 2017, 17/12/2017 [cited 2017 17/12/17]:[9 p.]. Available from: https://www.math.ubc.ca/~peirce/M406_Lecture_3_Runge_Phenomenon_Piecewise_Polynomial_Interpolation.pdf.

[21] D. Lewis, A. Micke, X. Yu, M.F. Chan, An efficient protocol for radiochromic film dosimetry combining calibration and measurement in a single scan, Med. Phys. 39 (10) (2012) 6339−6350.

[22] S. Devic, J. Seuntjens, G. Hegyi, E.B. Podgorsak, C.G. Soares, A.S. Kirov, et al., Dosimetric properties of improved GafChromic films for seven different digitizers, Med. Phys. 31 (9) (2004) 2392−2401.

[23] H. Alnawaf, P.K. Yu, M. Butson, Comparison of Epson scanner quality for radiochromic film evaluation, J. Appl. Clin. Med. Phys. 13 (5) (2012) 3957.

[24] M. Martisikova, B. Ackermann, O. Jakel, Analysis of uncertainties in Gafchromic EBT film dosimetry of photon beams, Phys. Med. Biol. 53 (24) (2008) 7013−7027.

 https://doi.org/10.1016/j.heliyon.2018.e00864

[25] S. Chiu-Tsao, G. Massillon-Jl, I. Domingo-Munoz, M. Chan, SU-E-T-96: energy dependence of the new GafChromic- EBT3 film's dose response-curve, Med. Phys. 39 (6 Part 11) (2012) 3724.

[26] A. Blair, J. Meyer, Characteristics of Gafchromic XR-RV2 radiochromic film, Med. Phys. 36 (7) (2009) 3050−3058.

[27] H. Alva, H. Mercado-Uribe, M. Rodriguez-Villafuerte, M.E. Brandan, The use of a reflective scanner to study radiochromic film response, Phys. Med. Biol. 47 (16) (2002) 2925−2933.

[28] R.V.K. Reddy, K.P. Raju, L.R. Kumar, M.J. Kumar, Grey level to RGB using YCbCr color space technique, Int. J. Comp. Appl. 147 (7) (2016).

[29] C. Rafael, R.E.W. Gonzalez, Digital Image Processing, second ed., Prentice Hall, Upper Saddle River, NJ, 2002, 793 p.

https://doi.org/10.1016/j.heliyon.2018.e00864